Title

Conformational dynamics of the Hop1 HORMA domain reveal a common mechanism with the spindle checkpoint protein Mad2

Journal

Nucleic Acids Research, 46(1)

ISSN

0305-1048

Authors

West, Alan MV
Komives, Elizabeth A
Corbett, Kevin D

Publication Date

2018-01-09

DOI

10.1093/nar/gkx1196

Peer reviewed

Published online 25 November 2017

Nucleic Acids Research, 2018, Vol. 46, No. 1 ***279–292***
doi: 10.1093/nar/gkx1196

Conformational dynamics of the Hop1 HORMA domain reveal a common mechanism with the spindle checkpoint protein Mad2

Alan M.V. West[1,2], Elizabeth A. Komives[3] and Kevin D. Corbett[1,3,4,*]

[1]Ludwig Institute for Cancer Research, San Diego Branch, La Jolla, CA 92093, USA, [2]Biomedical Sciences Graduate Program, University of California, San Diego, La Jolla, CA 92093, USA, [3]Department of Chemistry and Biochemistry, University of California, San Diego, La Jolla, CA 92093, USA and [4]Department of Cellular and Molecular Medicine, University of California, San Diego, La Jolla, CA 92093, USA

Received August 03, 2017; Revised November 13, 2017; Editorial Decision November 14, 2017; Accepted November 16, 2017

ABSTRACT

The HORMA domain is a highly conserved protein–protein interaction module found in eukaryotic signaling proteins including the spindle assembly checkpoint protein Mad2 and the meiotic HORMAD proteins. HORMA domain proteins interact with short 'closure motifs' in partner proteins by wrapping their C-terminal 'safety belt' region entirely around these motifs, forming topologically-closed complexes. Closure motif binding and release requires large-scale conformational changes in the HORMA domain, but such changes have only been observed in Mad2. Here, we show that *Saccharomyces cerevisiae* Hop1, a master regulator of meiotic recombination, possesses conformational dynamics similar to Mad2. We identify closure motifs in the Hop1 binding partner Red1 and in Hop1 itself, revealing that HORMA domain–closure motif interactions underlie both Hop1's initial recruitment to the chromosome axis and its self-assembly on the axis. We further show that Hop1 adopts two distinct folded states in solution, one corresponding to the previously-observed 'closed' conformation, and a second more extended state in which the safety belt region has disengaged from the HORMA domain core. These data reveal strong mechanistic similarities between meiotic HORMADs and Mad2, and provide a mechanistic basis for understanding both meiotic chromosome axis assembly and its remodeling by the AAA+ ATPase Pch2/TRIP13.

INTRODUCTION

Meiosis is a specialized two-stage cell division program that gives rise to haploid gametes in sexually reproducing organisms. After a single round of DNA replication, homologous chromosomes segregate from one another in meiosis I, and sister chromosomes subsequently segregate in meiosis II. The extended prophase of meiosis I, in which homologs identify and physically associate with one another through a modified homologous recombination pathway, is governed by a conserved meiosis-specific protein assembly called the chromosome axis. The axis organizes each pair of sister chromosomes as a linear array of chromatin loops and promotes DNA double-strand break (DSB) formation by the conserved Spo11 endonuclease (1,2). After DSB formation, axis proteins suppress repair of these DSBs via the nearby sister chromosome, thereby promoting repair via the homolog (3–8). This preference is key for the formation of crossovers (COs) that enable homologs to bi-orient on the meiosis I spindle, then properly segregate from one another to reduce ploidy by half. In late prophase, the synaptonemal complex assembles along the length of paired homologs' chromosome axes, bringing the homologs into close juxtaposition and promoting the final steps of crossover formation (reviewed in (9,10)). In many organisms including the budding yeast *Saccharomyces cerevisiae*, plants, and mammals, synaptonemal complex assembly is coordinated with remodeling of the chromosome axis (11–14). By depleting CO-promoting factors from homolog pairs that have properly associated, this axis remodeling process constitutes a feedback mechanism governing CO levels on a per-chromosome basis (15,16).

The chromosome axis is highly conserved in eukaryotes. Major axis components include cohesin complexes containing at least one meiosis-specific subunit, the kleisin Rec8 (17–21); one or more proteins of the meiotic HORMA-domain containing (HORMAD) protein family (discussed further below); and in most organisms a coiled-coil domain-containing 'linker' protein (*S. cerevisiae* Red1, *S. pombe* Rec10, mammalian SYCP2/SYCP3 and plant ASY3) required for localization of HORMADs (22–28). In the budding yeast *S. cerevisiae*, the axis comprises Rec8-containing

*To whom correspondence should be addressed. Tel: +1 858 534 7267; Fax: +1 858 534 7750; Email: kcorbett@ucsd.edu

cohesin complexes and the HORMAD protein Hop1, plus the linker protein Red1 (28–32). In wild-type cells, Red1's distribution on chromosomes largely mirrors that of meiotic cohesin complexes (31), suggesting that Red1 may associate directly with cohesins. Red1 has also been shown to bind directly to Hop1 both *in vitro* and in cells (24,33), and is required for normal chromosome localization of Hop1 (28,31), suggesting a hierarchical cohesin→Red1→Hop1 axis assembly mechanism. Hop1, Red1, and Rec8 are all required for normal numbers and spatial distribution of meiotic DSBs (34–36), acting at least in part to recruit the Rec114:Mei4:Mer2 complex to the chromosome axis (29). These proteins are, in turn, required for Spo11 recruitment to the axis and for DSB formation (37–42). After DSBs have formed, Hop1 is phosphorylated by the DNA damage-response kinases Mec1 and Tel1 (homologs of mammalian ATM and ATR) in its SCD region (SQ/TQ Cluster Domain), particularly residues S298 and T318 (5,43). This phosphorylation promotes the recruitment and activation of the Mek1 kinase, which biases repair of DSBs toward the homolog instead of the sister chromosome, thereby generating COs (6,44–46). After CO designation and the initiation of synaptonemal complex assembly, Hop1 is thought to be removed from the chromosome axis through the action of the conserved AAA+ ATPase Pch2 (13,47,48). As chromosome-localized Hop1 promotes both DSB and CO formation, its removal constitutes a feedback mechanism suppressing further recombination on chromosomes/regions that have already obtained COs (13,49). Many of Hop1's regulatory functions are shared by its orthologs in other eukaryotes, including promoting DSBs and biasing their repair toward the homolog, and removal from the chromosome axis by Pch2 (TRIP13 in mammals) in coordination with synaptonemal complex assembly (11,14,50–52).

Hop1 is the founding member of the meiotic HORMAD protein family, which also includes *S. pombe* Hop1, plant ASY1/ASY2, mammalian HORMAD1/HORMAD2 and *Caenorhabditis elegans* HIM-3/HTP-1/HTP-2/HTP-3 (11,27,50,53–56). The meiotic HORMADs share a peptide-binding domain termed the HORMA domain, named for three functionally-diverse protein families originally shown to share it: Hop1, Rev7 and Mad2 (57,58). The best-understood HORMA domain protein is Mad2, a key regulator of the mitotic spindle assembly checkpoint. This checkpoint monitors kinetochore-microtubule attachments in mitosis and meiosis, and delays anaphase onset until all kinetochores are properly attached to spindle microtubules (59–61). The Mad2 HORMA domain can adopt two distinct stably folded conformations, termed 'open' (O-Mad2) and 'closed' (C-Mad2) (62–64). In the closed conformation, Mad2 binds short peptides called 'Mad2-interacting motifs' (MIMs) or, more generally, 'closure motifs' (65–67). The two conformations of Mad2 differ mainly in the location and conformation of its C-terminal 'safety belt' region: in O-Mad2, this region is stably folded against the closure motif binding site (β-strand 6), preventing closure motif binding (68). In C-Mad2, the safety belt is disengaged from this site, allowing a closure motif to bind strand β6. The safety belt in turn translocates to the opposite side of the HORMA domain (strand β5), wrapping around the ligand to create a topological link between HORMA domain and closure motif (66,67,69). Coupled to safety belt motions are changes in the domain's N-terminus: in O-Mad2, the N-terminus associates with strand β5 to stabilize the open conformation. In C-Mad2, however, this region dissociates from the HORMA domain core and is mostly disordered. In the spindle assembly checkpoint, Mad2 is recruited to unattached kinetochores via a closure motif on its binding partner Mad1 (67,70). This C-Mad2 in turn recruits soluble O-Mad2, forming a pseudo-symmetric C-Mad2:O-Mad2 dimer via a conserved surface opposite the closure motif binding site (69,71). Mad2 dimerization promotes conversion of O-Mad2 to the closed state and binding to a closure motif in Cdc20, to form the core of the mitotic checkpoint complex (72–74). Conformational conversion of Mad2 is believed to involve a transient high-energy state in which the safety belt has dissociated from the HORMA domain core, which allows closure motif binding followed by safety belt re-association to produce the C-Mad2:Cdc20 complex (62,63,75). Recently, Pch2/TRIP13 has also been implicated in the spindle assembly checkpoint pathway, acting with an adapter protein, $p31^{comet}$, to disassemble the MAD2:Cdc20 complex upon checkpoint silencing (76–82).

The close evolutionary relationship between Mad2 and the meiotic HORMADs, plus the involvement of a shared ATPase regulator, Pch2/TRIP13, strongly suggests mechanistic commonalities between these two protein families. Recently, we showed that the *C. elegans* meiotic HORMADs interact through association of their N-terminal HORMA domains with conserved closure motifs at their C-termini, and that the resulting hierarchical complex is essential for proper regulation of CO formation and chromosome segregation (83). We further identified closure motifs in the C-termini of the mammalian meiotic HORMADs, and demonstrated binding of these motifs to the HORMAD1 HORMA domain (83). In *S. cerevisiae*, prior genetic evidence has demonstrated the importance of both its N-terminal HORMA domain and a short, highly-conserved C-terminal region (46,84,85). These features, plus additional evidence of Hop1 self-association *in vitro* (86), suggest that Hop1 may also self-assemble through HORMA domain–closure motif interactions. Importantly, there is currently no evidence for homodimerization of meiotic HORMADs (58), suggesting that these proteins' assembly mechanisms are distinct from those of Mad2. Thus, the question of how meiotic HORMADs' HORMA domain conformation and closure motif binding activities are controlled remains an important question. Specifically, as meiotic HORMADs have only been observed in their closed, closure-motif bound conformation, it is not known whether they adopt an 'open' conformation similar to Mad2 during closure motif binding and dissociation. Indeed, no HORMA domain protein other than Mad2 has been shown to possess the conformational dynamics that would seem to be necessary for assembly and disassembly of HORMA domain–closure motif complexes. Another major question is how meiotic HORMADs are initially recruited to the chromosome axis by coiled-coil 'linker' proteins such as Red1, and whether this recruitment also involves HORMA domain–closure motif interactions.

Here, we present a detailed biophysical characterization of the *S. cerevisiae* Hop1 HORMA domain. We identify related motifs in the Hop1 C-terminus and in Red1 that bind the Hop1 HORMA domain, indicating that HORMA domain–closure motif interactions are responsible for both initial localization and self-assembly of Hop1 on the chromosome axis. We further find that the Hop1 HORMA domain displays conformational dynamics reminiscent of Mad2, and identify a new conformation of Hop1, termed 'unbuckled', that likely functions analogously to open Mad2. These results outline the assembly mechanisms of the meiotic chromosome axis and reveal a close structural and functional relationship between the meiotic HORMADs and Mad2.

MATERIALS AND METHODS

Protein expression and purification

Structural modeling. An initial structural model of the Hop1 HORMA domain was generated using the One-to-One Threading mode of the PHYRE2 server (http://www.sbg.bio.ic.ac.uk/~phyre2/) using *C. elegans* HTP-1 (PDB ID 4TZO, chain C) as a template (83), then this model was manually adjusted. Side chain rotamers were not modeled. Sequence similarity between closure motifs in *S. cerevisiae* Hop1/Red1 and *C. elegans* HORMADs is not high enough to accurately model the register of the closure motif peptide in this model.

Protein purification. Hop1$^{2–255}$ and Hop1$^{2–255}$ LL were expressed in *Escherichia coli* strain Rosetta 2 (DE3) pLysS (EMD Millipore, Billerica, MA, USA) at 20°C for 16 h, then cells were harvested by centrifugation and resuspended in buffer A (20 mM Tris pH 8.5, 10% glycerol) plus 300 mM NaCl, 10 mM imidazole and 2 mM β-mercaptoethanol. Protein was purified by Ni^{2+}-affinity (Ni-NTA agarose, Qiagen) and ion-exchange (Hitrap Q HP, GE Life Sciences, Piscataway, NJ, USA) chromatography. Tags were cleaved with TEV protease (87), and cleaved protein was passed over a size exclusion column (Superdex 200, GE Life Sciences) in buffer A plus 300 mM NaCl and 1 mM dithiothreitol (DTT). Full-length Hop1 (wild-type and K593A), Hop1$^{\Delta 584}$, and Red1$^{2–362}$ were purified as above, but at pH 7.5 instead of 8.5.

For size-exclusion chromatography coupled multi-angle light scattering (SEC-MALS), proteins were separated on a Superdex 200 Increase 10/300 GL size exclusion column (GE Life Sciences) in a buffer containing 20 mM HEPES pH 7.5, 300 mM NaCl, 10% glycerol, and 1 mM DTT. Absorbance was measured at 280 nm, and light scattering and refractive index profiles collected by miniDAWN TREOS and Optilab T-rEX detectors (Wyatt Technology, Santa Barbara, CA, USA), respectively, and their molecular weights calculated using ASTRA v. 6 software (Wyatt Technology). For size-exclusion chromatography +/– Red1$^{345–362}$ peptide, proteins were pre-incubated with a 2-fold molar excess of Red1$^{345–362}$ peptide for 30 min at 4°C, then separated on a Superdex 200 Increase 10/300 GL size exclusion column in a buffer containing 20 mM MES pH 6.0, 300 mM NaCl, 10% glycerol, and 1 mM DTT.

Protein interaction assays. Putative closure motifs in Hop1 (residues 584–605) and Red1 (residues 330–362), along with point-mutants, were cloned into a pET3a-based vector with an upstream Kozak sequence and N-terminal maltose binding protein (MBP) tag, and translated *in vitro* with a TNT T7 Transcription/Translation kit (Promega) with ^{35}S-methionine. Ni^{2+} pulldown assays were performed with C-terminally His_6-tagged Hop1$^{1–255}$. 10 μg purified bait protein was incubated with 10 μl of the translation reaction in binding buffer (20 mM HEPES, pH 7.5, 150 mM NaCl, 20 mM imidazole, 5% glycerol, 1 mM dithiothreitol (DTT), 0.1% NP-40) for 90 min at 4°C, then 15 μl Ni-NTA beads were added, and the mixture was incubated a further 45 min. Beads were washed three times with 0.5 ml buffer, then eluted with 25 μl elution buffer (2× SDS-PAGE loading dye plus 400 mM imidazole) and boiled. Samples were run on SDS-PAGE, then the gel was dried and scanned with a phosphorimager. For competition assays, fluorescein isothiocyanate (FITC)-labeled competitor peptides (Red1$^{330–362}$ (FEDEKLGETFFHNVNNIPKISEVQ NFLVLDYIE) and a sequence-scrambled version (NSVE NFIVEGLIFNDKLEPLFHYKDNEETVIQ) were added prior to addition of *in vitro*-translated protein, in 2-fold molar excess over bait protein.

Ni^{2+} pulldown assays were performed with purified His_6-MBP fused Red1$^{2–362}$ and Hop1$^{584–605}$. 50 μl reactions with 10 μg of bait protein plus 30 μg of prey protein (untagged full-length Hop1, Hop1 K593A, Hop1$^{2–255}$ or Hop1$^{2–255}$LL) in binding buffer (20 mM HEPES pH 7.5, 300 mM NaCl, 10 mM imidazole, 10% glycerol, 1 mM DTT, 0.1% NP-40) were incubated 2 hours at room temperature. Samples were then mixed with 20 ul of magnetic Ni-NTA beads (5% suspension; Qiagen) and incubated with rotation for 30 min. Beads were washed three times with 0.5 ml binding buffer, eluted with 25 μl of elution buffer (2x SDS-PAGE loading dye plus 400 mM imidazole) then boiled. Samples were analyzed by SDS-PAGE, and visualized by Coomassie Blue staining.

For fluorescence polarization peptide binding assays, FITC-labeled peptides (BioMatik) at 50 nM were incubated with 12 nM–100 μM Hop1$^{2–255}$ or Hop1$^{2–255}$LL in 50 μl binding buffer for 30 min, then transferred to a 384-well black plate. Fluorescence polarization of triplicate reactions were read using a Tecan Infinite M1000 PRO fluorescence plate reader, and binding data were analyzed with Graphpad Prism v.6 using a single-site binding model.

Hydrogen–deuterium exchange mass spectrometry. HD exchange experiments were conducted with a Waters Synapt G2S system. 5 ul samples in exchange buffer (20 mM HEPES pH 7.5, 300 mM NaCl, 10% glycerol) were mixed with 55 μl of D_2O buffer for several deuteration times (10 s, 30 s, 1 min, 2 min, 5 min) at 15°C. The exchange was quenched for 2 min at 1°C with an equal volume of quench buffer (200 mM iodoacetic acid (IAA), 400 mM Tris–HCl pH 8.5, 6.2 M urea, 2 mM EDTA). A portion of the quenched sample (50 μl) was injected onto an in-line pepsin column (Applied Biosystems, Poroszyme Immobilized Pepsin cartridge). The resulting peptic peptides were then separated on a C18 column (Waters, Acquity UPLC BEH C18, 1.7 μm, 1.0 mm × 50 mm) fit with a Van-

guard trap column using a 3–85% acetonitrile (containing 0.1% formic acid) gradient over 12 min at a flow rate of 40 μl/min. The separated peptides were directed into a Waters SYNAPT G2s quadrupole time-of-flight (qTOF) mass spectrometer. The mass spectrometer was set to collect data in the MSE, ESI+ mode; in a mass acquisition range of m/z 255.00−1950.00; with a scan time of 0.4 s. Continuous lock mass correction was accomplished with infusion of the LeuEnk peptide every 30 s (mass accuracy of 1 ppm for the calibration standard). Peptides were identified using PLGS version 2.5 (Waters, Inc.). The relative deuterium uptake for each peptide was calculated by comparing the centroids of the mass envelopes of the deuterated samples with the undeu- terated controls using DynamX version 2.0 (Waters Corp.).

For analysis of peptides showing bimodal HD exchange behavior, assigned peaks for spectra collected at the 5-min time-point were exported as mass/charge versus intensity, normalized to a maximum intensity of 1.0 for each spectrum, and triplicate samples were fit in Graphpad Prism (version 6; Graphpad Software) to either a single Gaussian distribution:

$$Y = \text{Amplitude} * e^{-\frac{(X-\text{Mean})^2}{2*\text{StDev}^2}}$$

where Amplitude is the amplitude, Mean is the mean, and StDev is the standard deviation of the function, or a sum of two Gaussian distributions:

$$Y = \left(\text{Amplitude}_{\text{one}} * e^{-\frac{(X-\text{Mean}_{one})^2}{2*\text{StDev}_{\text{one}}^2}}\right) + \left(\text{Amplitude}_{\text{two}} * e^{-\frac{(X-\text{Mean}_{\text{two}})^2}{2*\text{StDev}_{\text{two}}^2}}\right)$$

where $\text{Amplitude}_{\text{one}}$, $\text{Mean}_{\text{one}}$and $\text{StDev}_{\text{one}}$ apply to the first Gaussian function, and $\text{Amplitude}_{\text{two}}$, $\text{Mean}_{\text{two}}$and $\text{StDev}_{\text{two}}$ apply to the second.

RESULTS

Hop1 and Red1 possess similar Hop1 HORMA domain-binding 'closure motifs'

To better understand the functional parallels between *S. cerevisiae* Hop1 and its orthologs in *C. elegans* and mammals, we first sought to determine if Hop1 self-assembles through interactions between its N-terminal HORMA domain and a C-terminal closure motif (83). Sequence alignments show that fungal Hop1 proteins share a highly conserved C-terminal Domain (CTD) of ∼20 amino acids (Figure 1A). Prior work has shown that deletion of the C-terminal 20 residues of Hop1, or mutation of the highly-conserved 'KIS' motif spanning residues 593–595 (K593A or S595N) dramatically reduces meiotic DSB and CO numbers and causes high spore lethality, indicating an important role for this domain in Hop1 function (46,85,88). We noticed that the Hop1 C-terminus bears limited sequence homology with a region of Red1 previously shown to interact directly with Hop1, notably including a 'KIS' motif spanning Red1 residues 348–350 (Figure 1A) (24). Further, a Red1 K348E mutant has previously been shown to eliminate its ability to bind Hop1, leading to reduced COs, defective homolog synapsis, and low spore viability (24). Together, the similarity of these motifs and their importance for axis structure and function suggest that both Hop1 and Red1 contain closure motifs that bind the Hop1 HORMA domain.

We defined the HORMA domain of *S. cerevisiae* Hop1 by modeling the structure of this domain onto on our prior structure of *C. elegans* HTP-1 (15% identity and 35% similarity to Hop1 in this domain) (Figure 1B, Supplementary Figure S1). We expressed and purified an isolated Hop1 HORMA domain construct ($\text{Hop1}^{2–255}$), and showed that this truncated construct as well as full-length Hop1 robustly bind purified $\text{Red1}^{1–362}$, which encompasses the conserved N-terminal domain of this protein plus the region previously shown to interact with Hop1 (Supplementary Figure S2). Because of high protease-sensitivity of purified full-length Red1, we were unable to demonstrate a direct interaction between purified full-length Hop1 and Red1 proteins.

We next tested binding of $\text{Hop1}^{2–255}$ to fluorescently-labeled peptides encoding residues 345–362 of Red1 and 584–605 of Hop1. We detected robust binding between $\text{Hop1}^{2–255}$ and the $\text{Red1}^{345–362}$ peptide (K_d = 340 nM), and weaker but detectable binding to the $\text{Hop1}^{584–605}$ peptide (K_d = 6 μM) (Figure 2A). In both cases, binding was abolished by point-mutations in the peptides based on previously identified mutations, Hop1 K593A and Red1 K348E (Figure 2A) (46). We next used a Ni^{2+} pulldown assay with His_6-tagged $\text{Hop1}^{2–255}$ and *in vitro*-translated $\text{Hop1}^{584–605}$ or $\text{Red1}^{345–362}$ (produced as maltose binding protein fusions). As in the prior assays, we observed binding of the Hop1 HORMA domain to both peptides, that was disrupted by mutation of the conserved lysine residue in the 'KIS' motif (Hop1 K593A/Red1 K348E) (Figure 2B). Moreover, binding of $\text{Hop1}^{584–605}$ to $\text{Hop1}^{2–255}$ was disrupted by addition of a two-fold molar excess of unlabeled $\text{Red1}^{345–362}$ peptide, revealing that the two putative closure motifs compete for a common binding site on the Hop1 HORMA domain (Figure 2B). Together, these data strongly suggest that Red1 and Hop1 possess similar HORMA domain-binding closure motifs. Further, Hop1 likely shares the propensity to self-associate through HORMA domain-CTD binding with its orthologs in *C. elegans* and mammals. When combined with prior data showing that the *hop1-K593A* mutation causes an 11-fold reduction in COs and results in high spore lethality (46), our data argues that Hop1 self-association at the meiotic chromosome axis is critically important for its regulatory functions.

As the Hop1 protein possesses a putative closure motif on its own C-terminus, this motif might be expected to compete for binding to peptides added in *trans*. To test this idea, we expressed and purified full-length Hop1, as well as variants with either the K593A mutation (Hop1^{K593A}) or with residues 585–605 in the CTD deleted ($\text{Hop1}^{\Delta 584}$), and tested their binding to the $\text{Red1}^{345–362}$ peptide. Compared to $\text{Hop1}^{2–255}$, we found that full-length Hop1 bound $\text{Red1}^{345–362}$ with dramatically lower affinity ($K_d = 2$ μM versus 340 nM for $\text{Hop1}^{2–255}$). In contrast, both Hop1^{K593A} (K_d = 51 nM) and $\text{Hop1}^{\Delta 584}$ (K_d = 450 nM) bound $\text{Red1}^{345–362}$ comparably to $\text{Hop1}^{2–255}$ (Figure 2C). Together, these data suggest that while Hop1's own CTD does compete with a

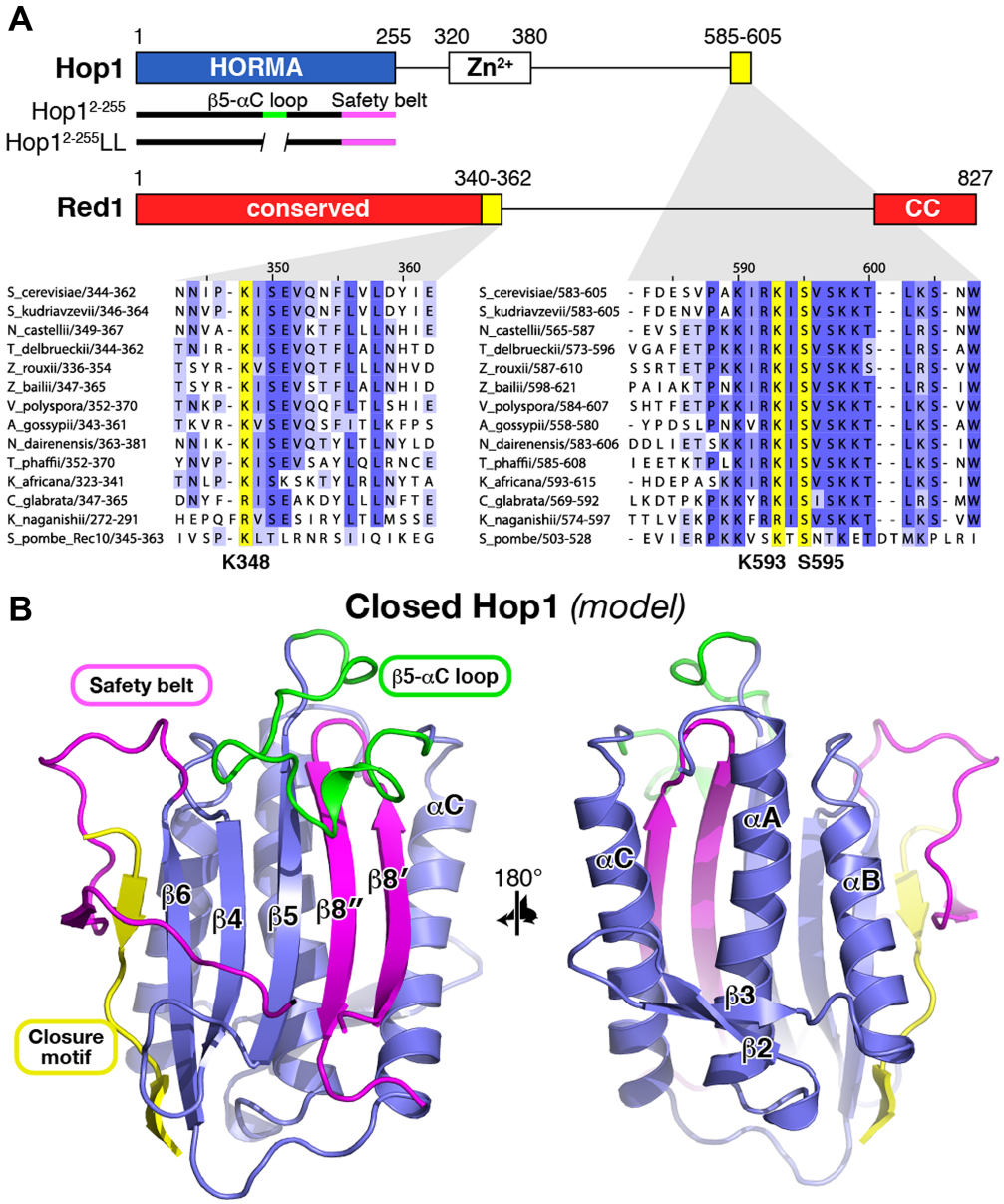

Figure 1. Hop1 and Red1 contain putative 'closure motifs' with similar sequence. (**A**) Domain diagrams of *S. cerevisiae* Hop1 and Red1, with known domains and domain boundaries marked (Zn^{2+}: Hop1 domain containing a conserved Cys4-His-Cys3 motif predicted to bind zinc; CC: Red1 predicted coiled-coil domain). Bottom: sequence alignment of putative closure motifs in Red1 and Hop1. (**B**) Structural model of the Hop1 HORMA domain, based on the structure of *C. elegans* HTP-1 bound to a closure motif from HIM-3 (PDB ID 4TZO; (83). For sequence alignment, see Supplementary Figure S1. The β5-αC loop (residues 135–158) replaced with GSG in $Hop1^{2–255}$ LL is shown in green. The safety belt region is shown in magenta, and the bound closure motif is shown in yellow.

Red1 peptide added in trans for HORMA domain binding, the higher affinity of Red1 for the Hop1 HORMA domain nonetheless likely enables Red1 to recruit full-length Hop1 directly to the chromosome axis.

The Hop1 HORMA domain adopts two distinct conformations in solution

During the purification of $Hop1^{2–255}$, we noticed that the protein elutes from a size-exclusion column as two closely-spaced peaks, one with an elution volume consistent with a compact monomer and the other consistent either with a dimer or an extended monomer (Figure 3A). Further analysis by size exclusion chromatography coupled to multi-angle light scattering (Figure 3B) showed that both peaks contain monomeric $Hop1^{2–255}$, demonstrating that the domain can likely adopt two different conformations in solution: one compact, and one more extended. We wondered how these two conformations of $Hop1^{2–255}$ might relate to the previously-described 'closed' and 'open' states of Mad2. We found that pre-incubation of $Hop1^{2–255}$ with the $Red1^{330–362}$ peptide shifted the equilibrium toward the later-eluting, more-compact size exclusion peak (Figure 3A). This finding suggests that the more-compact peak represents 'closed'

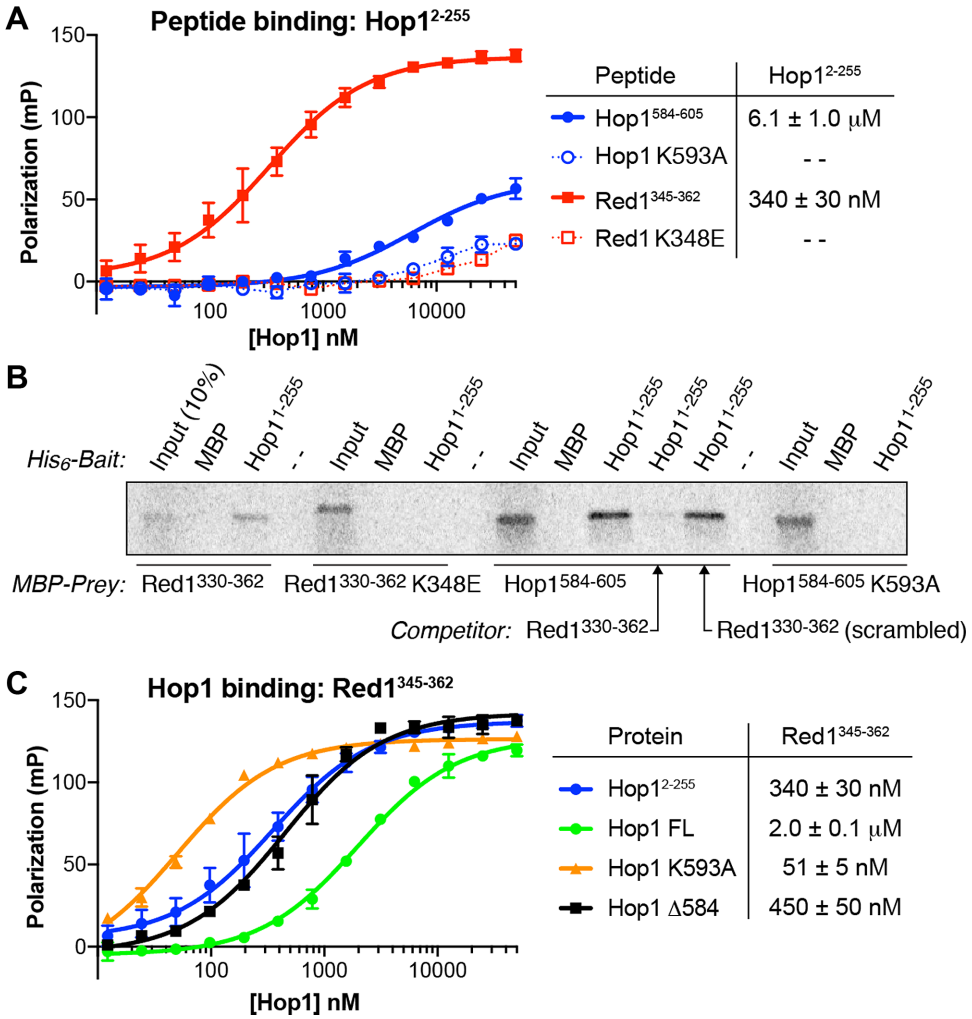

Figure 2. Closure motif peptide binding by Hop1. (**A**) Fluorescence polarization binding assays for Hop1$^{2–255}$ with four peptides: Hop1$^{584–605}$ (blue, K_d = 6.1 ± 1 μM), Hop1$^{584–605}$ K593A (dotted blue, K_d could not be fit), Red1$^{345–362}$ (red, K_d = 340 ± 30 nM) and Red1$^{345–362}$ K348E (dotted red, K_d could not be fit). Error bars indicate standard deviation from triplicate measurements. (**B**) Ni^{2+}-pulldown assay with His_6-tagged bait MBP (maltose binding protein; negative control) or Hop1$^{1–255}$ (C-terminal tag) and *in vitro*-translated MBP-fused Red1$^{330–362}$, Red1$^{330–362}$ K348E, Hop1$^{584–605}$, and Hop1$^{584–605}$ K593A. Competitor peptides were added at a two-fold molar excess over bait protein. (**C**) FP Binding assay for Red1$^{345–362}$ binding Hop1$^{2–255}$ (blue, K_d = 340 ± 30 nM), full-length Hop1 (green, K_d = 2.0 ± 0.1 μM), K593A (orange, K_d = 51 ± 5 nM), Δ584 (black, K_d = 450 ± 50 nM). See Supplementary Figure S2 for Ni^{2+} pulldown assays of Hop1 binding Red1$^{1–362}$ and Hop1$^{584–605}$.

Hop1 HORMA domain, and that the earlier-eluting, less-compact peak represents a second, potentially open-like conformation. Consistent with the idea that the HORMA domain of full-length Hop1 can associate with its own C-terminal tail, we fund that full-length Hop1 elutes from a size-exclusion column as a monomer (Figure 3B).

To further examine the conformational differences between the two states of the Hop1 HORMA domain, we generated several Hop1$^{2–255}$ variants based on mutations known to stabilize either the open or closed conformation of Mad2 (66,89,90), and examined their behavior in solution. While most variants destabilized Hop1$^{2–255}$, one markedly improved expression and stability of the protein. This mutant, referred to as 'loopless' or Hop1 LL (residues 135–158 replaced by a Gly-Ser-Gly linker), is based on the Mad2 'loopless' construct in which the extended β5-αC loop is replaced by a short linker (69). This mutation is thought to inhibit O-Mad2 to C-Mad2 conversion by preventing dissociation of the protein's N-terminus from the β5 strand, thereby disallowing safety belt movement and conversion to the C-Mad2 state. The structural effect of this mutant in Hop1 is difficult to predict, as the β5-αC loop is longer and more well-ordered in meiotic HORMADs than in Mad2, draping over the safety belt β-strands 8′ and 8″ (Figure 1B) (83). We found that in contrast to wild-type Hop1$^{2–255}$, Hop1$^{2–255}$LL migrated as a single species on a size-exclusion column consistent with a compact monomer, and that its elution profile was mostly unaffected by addition of the Red1$^{330–362}$ peptide (Figure 3A, B). We next tested binding of Hop1$^{2–255}$LL to the putative closure motif peptides Hop1$^{584–605}$ and Red1$^{345–362}$, and found that the mutated protein robustly binds both peptides; indeed, the loopless mutation seems to subtly increase peptide binding affinity compared to unmutated Hop1$^{2–255}$ (Figure 3C).

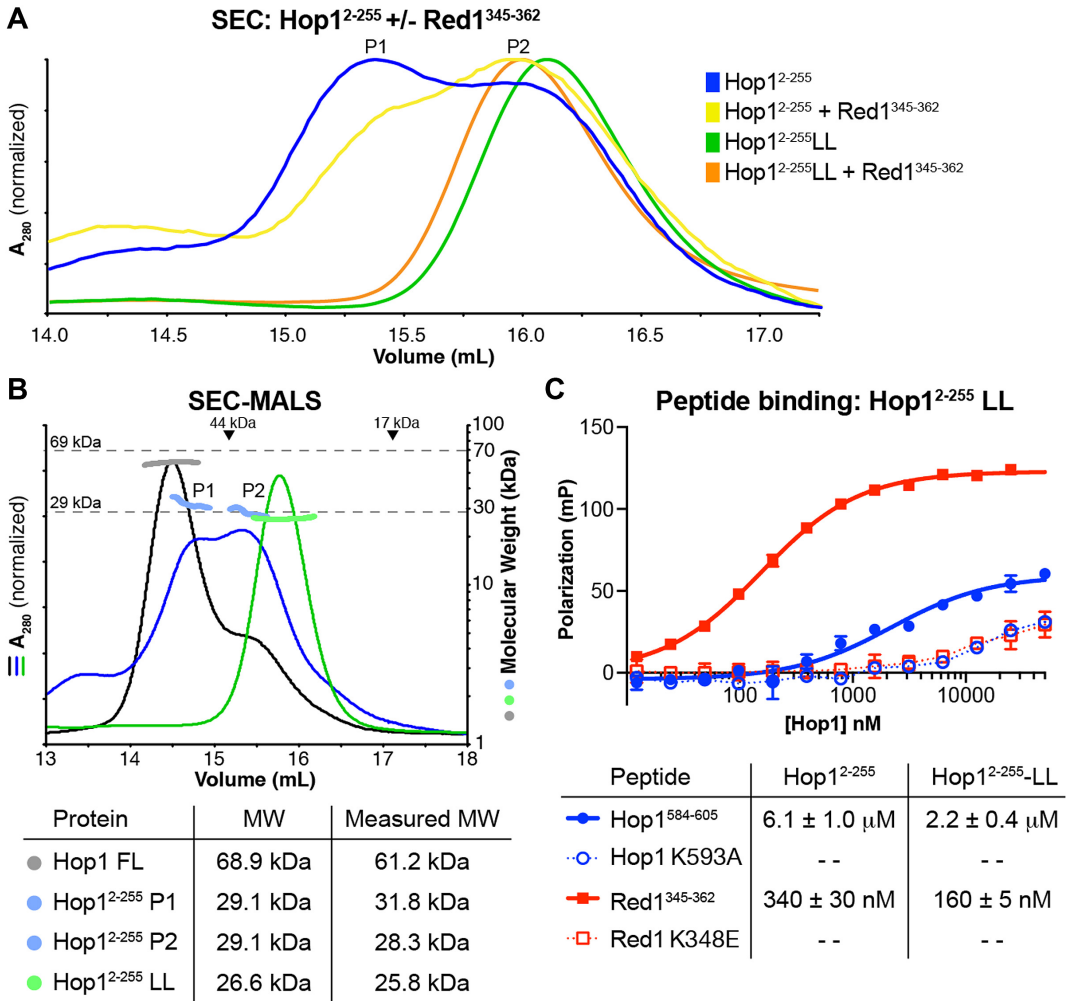

Protein	MW	Measured MW
Hop1 FL	68.9 kDa	61.2 kDa
Hop1 2-255 P1	29.1 kDa	31.8 kDa
Hop1 2-255 P2	29.1 kDa	28.3 kDa
Hop1 2-255 LL	26.6 kDa	25.8 kDa

Peptide	Hop1 2-255	Hop1 2-255-LL
Hop1 584-605	6.1 ± 1.0 μM	2.2 ± 0.4 μM
Hop1 K593A	- -	- -
Red1 345-362	340 ± 30 nM	160 ± 5 nM
Red1 K348E	- -	- -

Figure 3. The Hop1 HORMA domain shows two-state behavior in solution. (**A**) Size exclusion chromatography of Hop1$^{2–255}$ alone (blue), Hop1$^{2–255}$+Red1$^{330–362}$ (yellow), Hop1$^{2–255}$LL alone (green), and Hop1$^{2–255}$LL:Red1$^{330–362}$ (orange). (**B**) Size exclusion chromatography/multi-angle light scattering (SEC-MALS) analysis of full-length Hop1 (absorbance at 280 nm in black, measured molecular weight in grey), Hop1$^{2–255}$ (blue, two peaks defined as P1 and P2) and Hop1$^{2–255}$LL (green). *Below:* calculated and measured molecular weights for all constructs. (**C**) FP Binding assay for Hop1$^{2–255}$ LL binding putative closure motif peptides Hop1$^{584–605}$ (blue), Hop1$^{584–605}$ K593A (dashed blue), Red1$^{345–362}$ (red), and Red1$^{345–362}$ K348E (dashed red). Error bars indicate standard deviation from triplicate measurements. *Below:* Peptide-binding K_d's for Hop1$^{2–255}$ (from Figure 2A) and Hop1$^{2–255}$LL.

As the putative closure-motif binding site of Hop1 is not altered in this mutant, we interpret this slightly-increased affinity as indicating that the loopless mutation stabilizes the peptide-binding conformation of the Hop1 HORMA domain; namely, the 'closed' conformation.

Conformational dynamics of the Hop1 HORMA domain revealed by hydrogen-deuterium exchange mass spectrometry

We next sought further structural insight into the relationship between Hop1 HORMA domain conformation and peptide binding. As we were unable to identify crystallization conditions for the Hop1 HORMA domain or its complex with the Red1 closure motif, and low expression levels prevented examination by NMR, we instead turned to hydrogen-deuterium exchange mass spectrometry (HDX-MS). In HDX-MS, exchange of backbone amide hydrogen atoms with deuterium from D_2O-containing buffer provides information on the solvent-accessibility and secondary structure of different regions of a protein. We detected mass spectra for a set of common peptides in Hop1$^{2–255}$ and Hop1$^{2–255}$LL (covering 61% and 70% of the two constructs, respectively), including the C-terminal safety belt region but notably excluding the β5-αC loop (deleted in the Hop1 LL mutant, and not detected in Hop1$^{2–255}$) and the N-terminus (Supplementary Figure S3A and B). The rates of deuterium uptake in different regions largely agreed with predicted secondary structure in our model of the Hop1 HORMA domain based on *C. elegans* HTP-1 in the 'closed' conformation (Supplementary Figure S3C and D) (83). This was especially true for Hop1$^{2–255}$LL, which our size-exclusion chromatography analysis shows adopts exclusively the more-compact conformation.

We next compared HDX-MS profiles of Hop1$^{2–255}$ and Hop1$^{2–255}$LL in the absence and presence of the Red1$^{345–362}$ peptide. We found that all regions of Hop1$^{2–255}$ become more protected from H-D exchange in the presence of Red1$^{345–362}$ (Supplementary Figure S4A). Supporting our

assignment of Red1$^{345–362}$ as a closure motif, Hop1$^{2–255}$ regions predicted to lie adjacent to the closure motif binding site, including residues 182–195 and 198–211, are the most protected upon Red1$^{345–362}$ binding (Figure 4A, D, E). Residues 91–99 in helix αB, which is positioned just behind the closure motif binding site, as well as residues 74–90 in the β2-β3 hairpin adjacent to helix αB, also show a high degree of protection upon Red1$^{345–362}$ binding (Figure 4B and E). Finally, we also observed significant protection in regions corresponding to the β8′ and β8″ strands of the safety belt (residues 234–248), as well as helix αC (residues 164–173), which packs against these β-strands in the closed HORMA domain conformation (Figure 4C and E). Significant protection of the safety belt and adjacent regions upon binding of Red1$^{345–362}$ strongly suggests that the two Hop1 conformations we observe in solution differ largely in the conformation of the safety belt, consistent with the known conformational changes of Mad2.

In Hop1$^{2–255}$LL, H-D exchange rates for most regions, including peptides within and adjacent to the safety belt (residues 165–173 and 234–248), are much less affected by the addition of Red1$^{345–362}$ than in wild-type Hop1$^{2–255}$, supporting the idea that this mutant pre-forms the more-compact closed conformation in the absence of closure motif peptides (Figure 4C, Supplementary Figure S4B). Notable exceptions include residues 182–195 and 198–211, which make up the putative closure motif binding site: these regions would be expected to show different H-D exchange rates based on closure motif binding alone (Figure 4A and F). Thus, Hop1$^{2–255}$LL likely adopts an 'empty' closed conformation, to which closure motif peptides can directly associate without HORMA domain conformational conversion.

Our size-exclusion chromatography data showed that in the absence of a bound peptide, Hop1$^{2–255}$ adopts two different conformations in solution. Consistent with this finding, a number of peptides in the Hop1$^{2–255}$ construct show a bimodal distribution of H-D exchange rates (Figure 5). Bimodal H-D exchange rate distributions arise when the region in question can stably adopt two differently solvent-exposed conformations, resulting in high-exchanging (more solvent-exposed) and low-exchanging (less solvent-exposed) populations. The regions showing the most pronounced bimodality include residues 234–248, spanning β8′ and β8″ in the safety belt (Figure 5B), residues 164–173 in the adjacent αC-helix (Figure 5C), and residues 40–49 and 74–90 in the β2-β3 hairpin (Figure 5D-F). These peptides' bimodal behavior is nearly eliminated in the presence of the Red1$^{345–362}$ peptide, and they all show a monomodal H-D exchange rate distribution in Hop1$^{2–255}$LL regardless of Red1$^{345–362}$ binding (Figure 5A–C). Taken together, our HDX-MS data as a whole supports our identification of two stable conformations of the Hop1 HORMA domain, and suggest that the two states differ largely in the conformation of the domain's C-terminal safety belt region. While the strong bimodality in H-D exchange rates in these regions of wild-type Hop1$^{2–255}$ shows that this construct populates both states in solution, addition of the Red1$^{345–362}$ peptide shifts the equilibrium strongly in favor of the 'closed' conformation (Figure 5G). Hop1$^{2–255}$LL shows a strong bias toward the closed state on its own, which is further shifted toward this state upon binding the Red1$^{345–362}$ peptide.

DISCUSSION

In this study, we present a combined biochemical and biophysical characterization of the *S. cerevisiae* meiotic HORMA domain protein Hop1, identifying Hop1-binding closure motifs in both Hop1 and its binding partner Red1, and characterizing two distinct conformations of the Hop1 HORMA domain. When combined with prior genetic data, our results strongly suggest that HORMA domain–closure motif interactions underlie both the initial association and self-assembly of Hop1 on meiotic chromosomes. As both *C. elegans* and mammalian meiotic HORMADs self-assemble through HORMA domain–closure motif interactions (83), and most eukaryotes possess a Red1-like 'linker' protein required for axis assembly, our results suggest that initial association of meiotic HORMADs with meiotic chromosomes may also be mediated by HORMA domain–closure motif interactions. In *C. elegans*, our earlier work suggested that HTP-3 may bind directly to a subunit of the cohesin complex (83). Mammalian HORMAD1 and HORMAD2 may also bind cohesin complexes directly, or alternatively bind a closure motif in SYCP2 or SYCP3, in a parallel of the Hop1-Red1 association (22,91).

Our data suggest that Hop1 initially binds chromosomes through a closure motif in Red1, followed by additional Hop1 recruitment via head-to-tail oligomerization (Figure 6A). The competition we observe between Red1 and Hop1's own C-terminus for binding the HORMA domain suggests that in solution, Hop1 tends to form a 'self-closed' state but that recruitment of Hop1 to the chromosome axis by Red1 displaces the Hop1 CTD from the HORMA domain. This free CTD may in turn bind the HORMA domain of a second Hop1 monomer, initiating multimeric assembly. A conceptual problem with this model is that if the Hop1 HORMA domain can interact with a closure motif at its own C-terminus, the high local concentration of this closure motif would be expected to preclude binding to a second Hop1 monomer in trans. Hop1 oligomerization on the axis would only be favored if steric constraints not present in our reconstituted system were to inhibit self-interaction relative to oligomerization. Such constraints could include post-translational modifications and/or protein–protein interactions, such as the known phosphorylation of the Hop1 SCD region, which mediates recruitment of the Mek1 kinase (5,6,43,45,46). Pch2 may also contribute to Hop1 oligomerization (at least in some systems; see below), but its role is likely to be purely kinetic; that is, Pch2 could generally stimulate Hop1 conformational dynamics, but is unlikely to alter the equilibrium Hop1 oligomer length unless it is specifically localized to chromosomes (see below). While we are not yet able to explain the physical basis for Hop1 oligomerization, the strong effects on DSB and CO levels, homolog synapsis, and overall spore viability observed when mutating or deleting the Hop1 CTD (46,85) constitute strong indirect evidence that Hop1 oligomerization plays a key role in CO formation. Interestingly, the CO defect caused by a *hop1-K593A* mutant can be rescued by ectopic

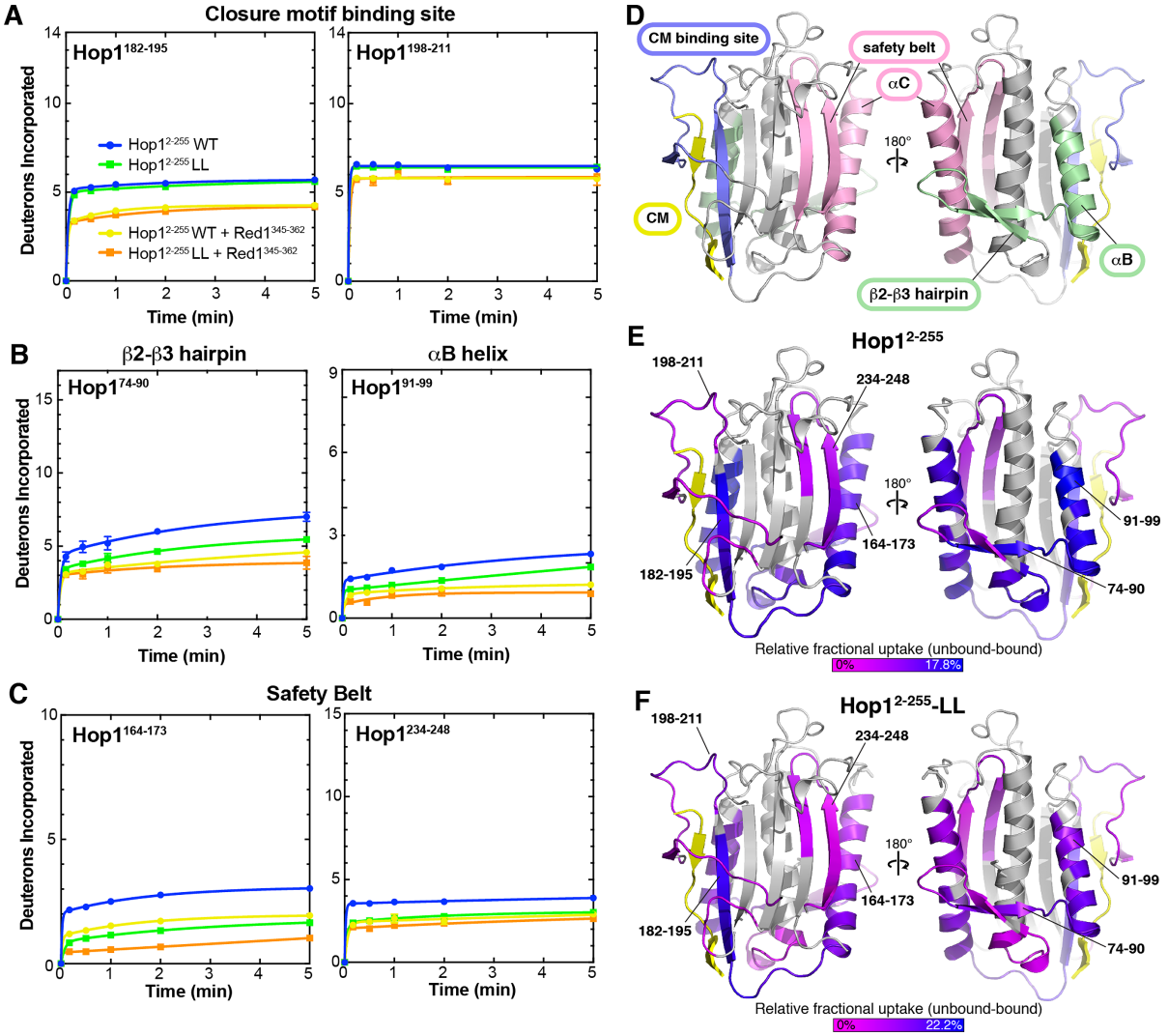

Figure 4. HD exchange in Hop1$^{2–255}$ and Hop1$^{2–255}$ LL. (**A**) Deuterium uptake plots of Hop1 residues 182–195 and 198–211, corresponding to the β6 strand and putative closure motif binding site, for Hop1$^{2–255}$ (blue, +Red$^{345–362}$ in yellow) and Hop1$^{2–255}$LL (green, +Red$^{345–362}$ in orange). (**B**) Uptake of residues 74–90 and 91–99, corresponding to the β2–β3 hairpin and helix αB. (**C**) Uptake of residues 164–173 and 234–248, corresponding to portions of the αC-helix and β8′-β8″ of the safety belt. See Supplementary Figure S3 for exchange data on all detected peptides. (**D**) Structural model of Hop1$^{2–255}$ showing regions described in panels (A–C): closure motif binding site (light blue), β2–β3 hairpin and helix αB (light green), and safety belt (pink). (**E**) Structural model of Hop1$^{2–255}$ colored according to the difference in relative deuterium uptake between the unbound and Red1$^{345–362}$ bound state. Magenta indicates no change in HD exchange rate, and blue indicates significantly less exchange (more protection) upon binding the closure motif peptide. Regions shown in gray were not detected. (**F**) Structural model of Hop1$^{2–255}$LL, showing protection upon binding Red1$^{345–362}$ as in panel (E). See Supplementary Figure S4 for exchange differences over time for Hop1$^{2–255}$ and Hop1$^{2–255}$LL ± Red1$^{345–362}$ peptide.

dimerization of Mek1, through its fusion to the dimeric glutathione S-transferase protein (46). This result suggests that one role of Hop1 self-association is to activate Mek1, likely by bringing multiple copies of the kinase into close proximity at the chromosome axis to enable trans-autoactivation (Figure 6A). Notably, the defect in both DSB and CO levels in a *hop1-K593A* strain is significantly less severe than in *hop1Δ*, and the Hop1 K593A mutant protein behaves well in vitro (this work) and localizes to meiotic chromosomes (46). These data support the idea that Red1 can recruit Hop1 directly, but that additional Hop1 recruitment through head-to-tail binding is nonetheless required to support wild-type levels of DSB formation and Mek1 kinase activation, which combine to support CO formation.

In addition to the meiotic HORMADs, HORMA domains are found in Mad2, Rev7, and two autophagy-related proteins, Atg13 and Atg101 (57,65). While Mad2 has been shown to adopt two stable conformations in solution, similar conformational dynamics have not been observed in any other HORMA domain protein family (65). Here, we show for the first time that the *S. cerevisiae* meiotic HORMAD Hop1 can adopt two different stable states in solution: a closed conformation similar to what we previously observed for the *C. elegans* meiotic HORMADs (83), and a more extended conformation. Our HDX-MS data indicate that the two states differ mainly in the conformation of the protein's C-terminal safety belt region, and that this region is probably disengaged from the HORMA domain core in the ex-

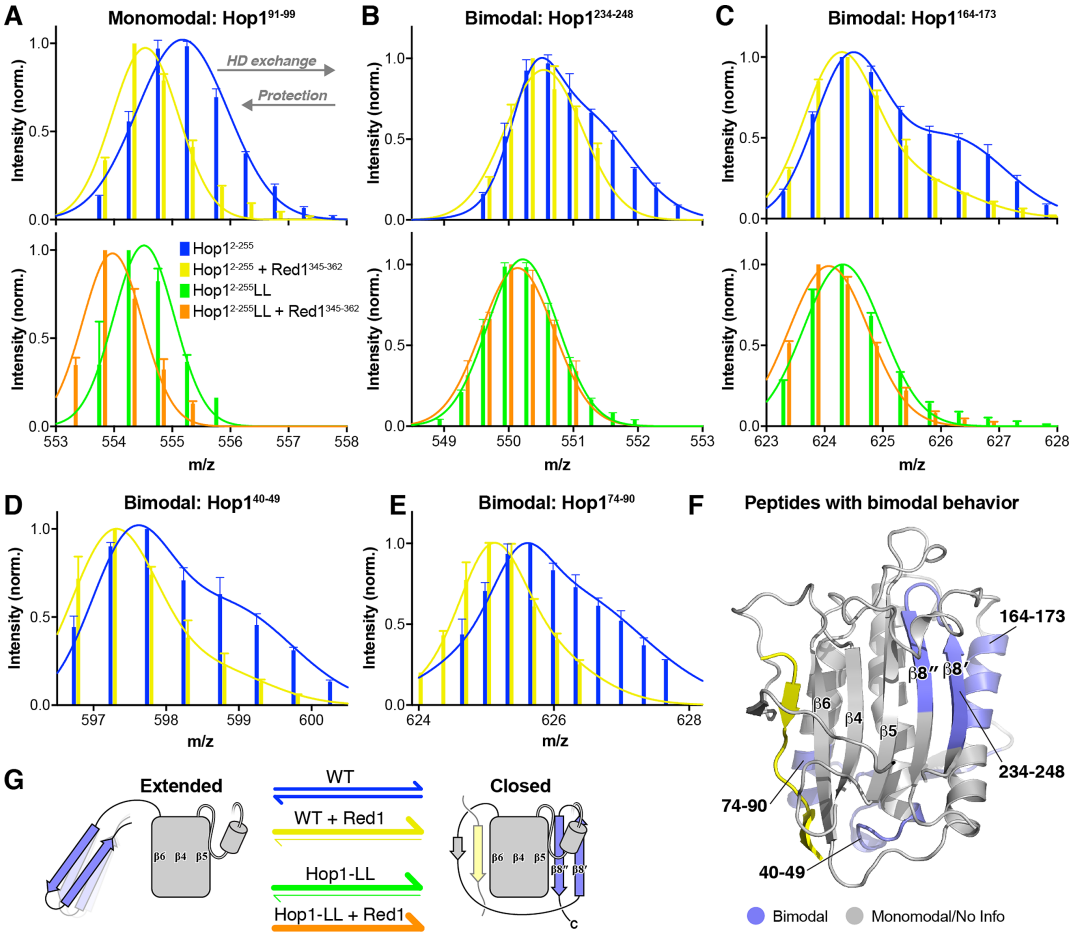

Figure 5. Bimodal HD exchange in Hop1$^{2–255}$. (**A**) Graphs showing normalized peak intensity versus mass/charge ratio (m/z) at 5 min exposure to D_2O for an example monomodal peptide, Hop1$^{91–99}$. *Top:* Hop1$^{2–255}$, alone (blue) and with Red1$^{345–362}$ (yellow). *Bottom:* Hop1$^{2–255}$ LL alone (green), and with Red1$^{345–362}$ (orange). Each dataset was fit to a single Gaussian distribution. (**B**) Graphs for Hop1$^{234–248}$ showing a bimodal distribution of HD exchange. Hop1$^{2–255}$ alone was fit to a sum of two Gaussian distributions, and the other three sampleswere fit to a single Gaussian distribution. (**C**) As (B), for Hop1$^{164-173}$. For this peptide, both Hop1$^{2–255}$ samples (with and without the Red1$^{345–362}$ peptide) were fit to a sum of two Gaussian distributions, while the Hop1$^{2-255}$ LL samples were fit to a single Gaussian distribution. (**D** and **E**) Graphs for Hop1$^{40–49}$ and Hop1$^{74–90}$, showing only data for Hop1$^{2–255}$ (data for Hop1$^{2–255}$ LL was not annotated well enough to fit). (**F**) Location of peptides showing bimodal HD exchange behavior (blue) on the modelled structure of Hop1$^{2–255}$ bound to a closure motif (yellow). (**G**) Schematic of proposed Hop1 HORMA domain equilibrium in four states. Hop1^{LL} (green) shows a strong bias toward the closed conformation compared to wild-type (blue), while addition of the Red1$^{345–362}$ peptide to either wild-type (yellow) or loopless Hop1 (orange), further shifts the equilibrium toward the closed conformation.

tended state. This model contrasts with Mad2's open conformation, in which the safety belt is stably associated with the closure-motif binding site, generating a structure that is similarly compact to the protein's closed conformation (92) (Figure 6B). The extended state of the Hop1 HORMA domain may therefore correspond more closely with the theorized transient Mad2 intermediate state, in which the safety belt has disengaged from the HORMA domain core to allow Cdc20 closure motif binding (62,69) (Figure 6B). Because the term 'intermediate' has more recently been used to refer to a compact Mad2 conformation adopted just prior to this conformational change (75), we instead introduce the term 'unbuckled' to refer to a HORMA domain conformation in which the safety belt is stably disengaged from the HORMA domain (Figure 6C).

While we designed the Hop1 'loopless' mutation based on a Mad2 variant that stabilizes this protein's open conformation (69), this mutation appears to stabilize the closed conformation in Hop1. In Mad2, truncation of the β5–αC loop is thought to disallow dissociation of the protein's N-terminal β1 strand from strand β5 in the HORMA domain core, thereby inhibiting the open-to-closed conformational change (69). We propose that Hop1 may not possess an N-terminal β1 strand, and that the 'unbuckled' conformation is instead stabilized by the extended β5-αC loop itself. As this loop is much longer in meiotic HORMADs than in Mad2 (24 residues in Hop1 versus 9 in Mad2), the loop could bind against β5 after safety belt dissociation to stabilize the unbuckled state. In this scheme, truncation of the β5-αC loop would be expected to destabilize the unbuckled state, thereby favoring the closed state as we observe for Hop1$^{2–255}$LL (Figure 6C). It is important to note that, while Hop1$^{2–255}$LL binds closure-motif peptides at least as tightly as wild-type Hop1$^{2–255}$, this mutant is likely to be strongly defective *in vivo*. As binding of a closure-motif peptide to an 'empty' closed Hop1 requires that the peptide thread un-

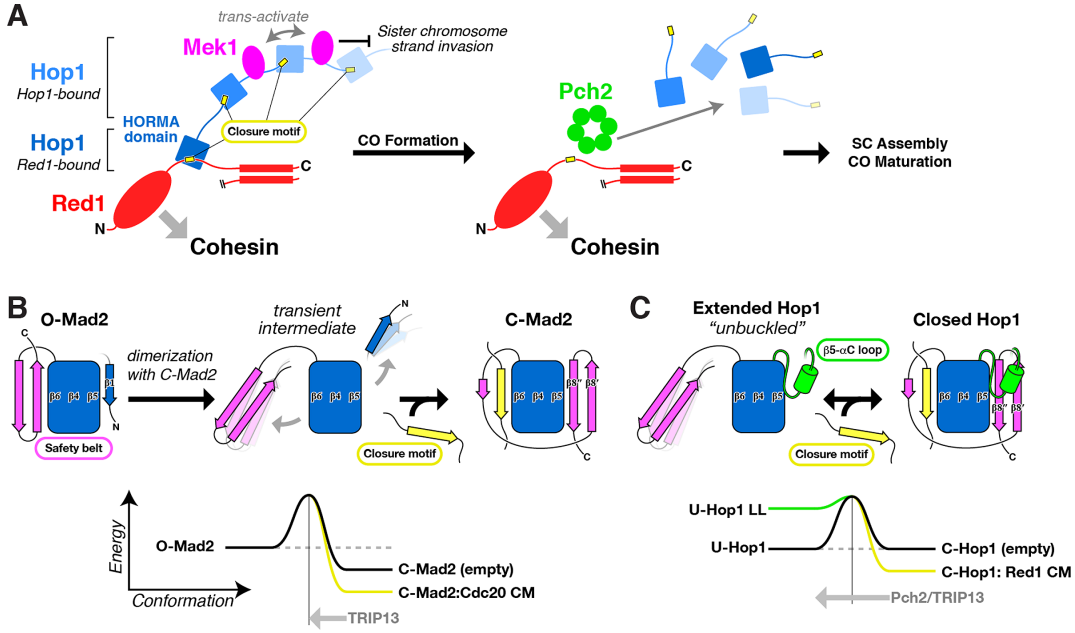

Figure 6. Model for Hop1 HORMA domain dynamics and meiotic chromosome axis assembly/disassembly. (**A**) Cartoon model of Hop1's recruitment, multimeric assembly, and disassembly along the chromosome axis. Hop1 (dark blue) is recruited to chromosomes by binding the Red1 closure motif (yellow). The displaced Hop1 CTD closure motif serves to recruit additional copies of Hop1 (lighter blue) to the chromosome axis. Hop1 oligomerization facilitates the trans-autoactivation of Mek1, resulting in a suppression of sister chromosome strand invasion and biasing DSB repair toward the homolog. After CO formation, Pch2 facilitates the removal of Hop1 from the axis by disrupting closure-motif interactions as the synaptonemal complex forms. (**B**) Cartoon representation and energy diagram of the Mad2 safety belt mechanism. The dimerization-stimulated conversion of O-Mad2 to C-Mad2, coupled to closure motif binding, requires dissociation of the N-terminus from the core of the HORMA domain and translocation of the safety belt (magenta). TRIP13 facilitates the conversion back to O-Mad2 by disengaging the safety belt from the HORMA domain core. (**C**) Cartoon representation and energy diagram of the proposed Hop1 safety belt mechanism. Closure motif binding stabilizes the closed state by promoting binding of the safety belt (magenta) to the HORMA domain core. The β5-αC loop (green) stabilizes the 'unbuckled' state through an unknown mechanism. Pch2/Trip13 promotes a closed-to-unbuckled conformational change of Hop1 by disengaging the safety belt from the HORMA domain core.

derneath part of the safety belt region, binding of the Red1 closure motif (more than 300 amino acids from either terminus of Red1) would be expected to require a conformational change in Hop1, much as in Mad2. We have so far been unable to test the function of Hop1 LL in *S. cerevisiae*, due to extremely poor expression of the mutant protein in meiotic cells. As Hop1$^{2–255}$LL is more highly expressed in *Escherichia coli* than the wild-type protein and is extremely stable in solution, the low levels of Hop1 LL we observe in *S. cerevisiae* may indicate that the protein is unstable, perhaps due to an inability to assemble on meiotic chromosomes.

Our data indicate that in *S. cerevisiae*, chromosome axis assembly is mediated in large part by binding of the Hop1 HORMA domain to closure motifs in both Hop1 and Red1. In contrast to Mad2, where assembly with Cdc20 occurs specifically at unattached kinetochores through dimerization-catalyzed conformational conversion, we envision meiotic chromosome axis assembly to be largely spontaneous. A major remaining question, however, is how meiotic HORMADs are removed from the chromosome axis by Pch2/TRIP13 in coordination with synaptonemal complex assembly (Figure 6A). We have recently shown that mammalian TRIP13 binds the disordered N-terminus of Mad2 and then partially unfolds the protein to mediate the disengagement of the Mad2 safety belt from the HORMA domain core (76,93). We further showed that N-terminal truncation of mouse HORMAD1 inhibits its TRIP13-mediated disassembly from meiotic chromosome axes, highlighting a common remodeling mechanism with Mad2 (93). We propose that Pch2/TRIP13 may be important to drive HORMA domain conformational dynamics and closure motif association/dissociation in meiotic HORMADs throughout eukaryotes. In this scheme, synaptonemal complex assembly likely triggers recruitment of Pch2/TRIP13 to the chromosome axis, where it removes HORMADs by disassembling HORMA domain–closure motif interactions. An important question in this regard is whether there exist two pools of meiotic HORMADs on chromosome axes, distinguished by their binding partners: in both *S. cerevisiae* and mammals, not all Hop1/HORMAD1 is removed from the axis upon synaptonemal complex assembly (11–13,28,94). This finding, plus the higher affinity of Hop1 for the Red1 closure motif and the location of the Red1 closure motif far from either terminus of this protein, suggests that Pch2 might more effectively disassemble Hop1–Hop1 complexes compared to Hop1–Red1 complexes.

In some systems, notably the rice *Oryza sativa*, mutation of Pch2/TRIP13 causes a loss of initial association of meiotic HORMADs with the chromosome axis (95). This observation suggests another potential role of Pch2/TRIP13, that also parallels earlier findings with Mad2. In the spindle assembly checkpoint, a pool of O-Mad2 is required

for kinetochore-recruitment and assembly with Cdc20, and TRIP13 is required to maintain this pool of O-Mad2 by converting empty C-Mad2 to the open conformation (76,96). In a similar vein, if the meiotic HORMADs in a given organism are much more stable in the closed conformation, Pch2/TRIP13 may be required to stimulate their dynamics to promote initial assembly of the chromosome axis, in addition to its later functions in HORMAD disassembly. Overall, the role of Pch2/TRIP13 in promoting function of meiotic HORMADs, and especially its detailed mechanism of meiotic HORMAD recognition and remodeling, will be an interesting avenue for future research.

SUPPLEMENTARY DATA

Supplementary Data are available at NAR Online.

ACKNOWLEDGEMENTS

The authors thank members of the Corbett lab for helpful discussions and critical reading of the manuscript, and E. Koslover for helpful discussions on Hop1 oligomerization.

FUNDING

UCSD Graduate Training Program in Molecular Biophysics [NIH T32 GM08326 to A.M.V.W.]; UCSD Academic Senate; Ludwig Institute for Cancer Research; National Institutes of Health [R01 GM104141 to K.D.C.]. Funding for open access charge: Ludwig Institute for Cancer Research.
Conflict of interest statement. None declared.

REFERENCES

1. Blat,Y., Protacio,R.U., Hunter,N. and Kleckner,N. (2002) Physical and functional interactions among basic chromosome organizational features govern early steps of meiotic chiasma formation. *Cell*, **111**, 791–802.
2. Keeney,S., Giroux,C.N. and Kleckner,N. (1997) Meiosis-specific DNA double-strand breaks are catalyzed by Spo11, a member of a widely conserved protein family. *Cell*, **88**, 375–384.
3. Hollingsworth,N.M. (2010) Phosphorylation and the creation of interhomolog bias during meiosis in yeast. *Cell Cycle*, **9**, 436–437.
4. Humphryes,N. and Hochwagen,A. (2014) A non-sister act: recombination template choice during meiosis. *Exp. Cell Res.*, **329**, 53–60.
5. Carballo,J.A., Johnson,A.L., Sedgwick,S.G. and Cha,R.S. (2008) Phosphorylation of the axial element protein Hop1 by Mec1/Tel1 ensures meiotic interhomolog recombination. *Cell*, **132**, 758–770.
6. Niu,H., Li,X., Job,E., Park,C., Moazed,D., Gygi,S.P. and Hollingsworth,N.M. (2007) Mek1 kinase is regulated to suppress double-strand break repair between sister chromatids during budding yeast meiosis. *Mol. Cell. Biol.*, **27**, 5456–5467.
7. Niu,H., Wan,L., Busygina,V., Kwon,Y., Allen,J.A., Li,X., Kunz,R.C., Kubota,K., Wang,B., Sung,P. *et al.* (2009) Regulation of meiotic recombination via Mek1-mediated Rad54 phosphorylation. *Mol. Cell*, **36**, 393–404.
8. Lao,J.P., Cloud,V., Huang,C.-C., Grubb,J., Thacker,D., Lee,C.-Y., Dresser,M.E., Hunter,N. and Bishop,D.K. (2013) Meiotic crossover control by concerted action of Rad51-Dmc1 in homolog template bias and robust homeostatic regulation. *PLoS Genet*., **9**, e1003978.
9. Zickler,D. and Kleckner,N. (2015) Recombination, Pairing, and Synapsis of Homologs during Meiosis. *Cold Spring Harb. Perspect. Biol.*, **7**, a016626.
10. Zickler,D. and Kleckner,N. (1999) Meiotic chromosomes: integrating structure and function. *Annu. Rev. Genet.*, **33**, 603–754.
11. Wojtasz,L., Daniel,K., Roig,I., Bolcun-Filas,E., Xu,H., Boonsanay,V., Eckmann,C.R., Cooke,H.J., Jasin,M., Keeney,S. *et al.* (2009) Mouse HORMAD1 and HORMAD2, two conserved meiotic chromosomal proteins, are depleted from synapsed chromosome axes with the help of TRIP13 AAA-ATPase. *PLoS Genet.*, **5**, e1000702.
12. Joshi,N., Barot,A., Jamison,C. and Börner,G.V. (2009) Pch2 links chromosome axis remodeling at future crossover sites and crossover distribution during yeast meiosis. *PLoS Genet.*, **5**, e1000557.
13. Börner,G.V., Barot,A. and Kleckner,N. (2008) Yeast Pch2 promotes domainal axis organization, timely recombination progression, and arrest of defective recombinosomes during meiosis. *Proc. Nat. Acad. Sci. U.S.A.*, **105**, 3327–3332.
14. Lambing,C., Osman,K., Nuntasoontorn,K., West,A., Higgins,J.D., Copenhaver,G.P., Yang,J., Armstrong,S.J., Mechtler,K., Roitinger,E. *et al.* (2015) *Arabidopsis PCH2* mediates meiotic chromosome remodeling and maturation of crossovers. *PLoS Genet.*, **11**, e1005372.
15. Thacker,D., Mohibullah,N., Zhu,X. and Keeney,S. (2014) Homologue engagement controls meiotic DNA break number and distribution. *Nature*, **510**, 241–246.
16. MacQueen,A.J. and Hochwagen,A. (2011) Checkpoint mechanisms: the puppet masters of meiotic prophase. *Trends Cell Biol.*, **21**, 393–400.
17. Lin,Y., Larson,K.L., Dorer,R. and Smith,G.R. (1992) Meiotically induced *rec7* and *rec8* genes of *Schizosaccharomyces pombe*. *Genetics*, **132**, 75–85.
18. Watanabe,Y. and Nurse,P. (1999) Cohesin Rec8 is required for reductional chromosome segregation at meiosis. *Nature*, **400**, 461–464.
19. Buonomo,S.B., Clyne,R.K., Fuchs,J., Loidl,J., Uhlmann,F. and Nasmyth,K. (2000) Disjunction of homologous chromosomes in meiosis I depends on proteolytic cleavage of the meiotic cohesin Rec8 by separin. *Cell*, **103**, 387–398.
20. Eijpe,M., Offenberg,H., Jessberger,R., Revenkova,E. and Heyting,C. (2003) Meiotic cohesin REC8 marks the axial elements of rat synaptonemal complexes before cohesins SMC1β and SMC3. *J. Cell Biol.*, **160**, 657–670.
21. Klein,F., Mahr,P., Galova,M., Buonomo,S.B.C., Michaelis,C., Nairz,K. and Nasmyth,K. (1999) A central role for cohesins in sister chromatid cohesion, formation of axial elements, and recombination during yeast meiosis. *Cell*, **98**, 91–103.
22. Offenberg,H.H., Schalk,J.A., Meuwissen,R.L., van Aalderen,M., Kester,H.A., Dietrich,A.J. and Heyting,C. (1998) SCP2: a major protein component of the axial elements of synaptonemal complexes of the rat. *Nucleic Acids Res.*, **26**, 2572–2579.
23. Rockmill,B. and Roeder,G.S. (1988) *RED1*: a yeast gene required for the segregation of chromosomes during the reductional division of meiosis. *Proc. Nat. Acad. Sci. U.S.A.*, **85**, 6057–6061.
24. Woltering,D., Baumgartner,B., Bagchi,S., Larkin,B., Loidl,J., de los Santos,T. and Hollingsworth,N.M. (2000) Meiotic segregation, synapsis, and recombination checkpoint functions require physical interaction between the chromosomal proteins Red1p and Hop1p. *Mol. Cell. Biol.*, **20**, 6646–6658.
25. Lammers,J.H., Offenberg,H.H., van Aalderen,M., Vink,A.C., Dietrich,A.J. and Heyting,C. (1994) The gene encoding a major component of the lateral elements of synaptonemal complexes of the rat is related to X-linked lymphocyte-regulated genes. *Mol. Cell. Biol.*, **14**, 1137–1146.
26. Lin,Y. and Smith,G.R. (1995) Molecular cloning of the meiosis-induced *rec10* gene of *Schizosaccharomyces pombe*. *Curr. Genet.*, **27**, 440–446.
27. Lorenz,A., Wells,J.L., Pryce,D.W., Novatchkova,M., Eisenhaber,F., McFarlane,R.J. and Loidl,J. (2004) *S. pombe* meiotic linear elements contain proteins related to synaptonemal complex components. *J. Cell Sci.*, **117**, 3343–3351.
28. Smith,A.V. and Roeder,G.S. (1997) The yeast Red1 protein localizes to the cores of meiotic chromosomes. *J. Cell Biol.*, **136**, 957–967.
29. Panizza,S., Mendoza,M.A., Berlinger,M., Huang,L., Nicolas,A., Shirahige,K. and Klein,F. (2011) Spo11-accessory proteins link double-strand break sites to the chromosome axis in early meiotic recombination. *Cell*, **146**, 372–383.
30. Klein,F., Mahr,P., Galova,M., Buonomo,S.B., Michaelis,C., Nairz,K. and Nasmyth,K. (1999) A central role for cohesins in sister chromatid cohesion, formation of axial elements, and recombination during yeast meiosis. *Cell*, **98**, 91–103.

31. Sun,X., Huang,L., Markowitz,T.E., Blitzblau,H.G., Chen,D., Klein,F. and Hochwagen,A. (2015) Transcription dynamically patterns the meiotic chromosome-axis interface. *eLife*, **4**, 8522.
32. de los Santos,T. and Hollingsworth,N.M. (1999) Red1p, a *MEK1*-dependent phosphoprotein that physically interacts with Hop1p during meiosis in yeast. *J. Biol. Chem.*, **274**, 1783–1790.
33. Hollingsworth,N.M. and Ponte,L. (1997) Genetic interactions between *HOP1*, *RED1* and *MEK1* suggest that *MEK1* regulates assembly of axial element components during meiosis in the yeast *Saccharomyces cerevisiae*. *Genetics*, **147**, 33–42.
34. Schwacha,A. and Kleckner,N. (1997) Interhomolog bias during meiotic recombination: meiotic functions promote a highly differentiated interhomolog-only pathway. *Cell*, **90**, 1123–1135.
35. Kugou,K., Fukuda,T., Yamada,S., Ito,M., Sasanuma,H., Mori,S., Katou,Y., Itoh,T., Matsumoto,K., Shibata,T. *et al.* (2009) Rec8 guides canonical Spo11 distribution along yeast meiotic chromosomes. *Mol. Biol. Cell*, **20**, 3064–3076.
36. Kim,K.P., Weiner,B.M., Zhang,L., Jordan,A., Dekker,J. and Kleckner,N. (2010) Sister cohesion and structural axis components mediate homolog bias of meiotic recombination. *Cell*, **143**, 924–937.
37. Li,J., Hooker,G.W. and Roeder,G.S. (2006) *Saccharomyces cerevisiae* Mer2, Mei4 and Rec114 form a complex required for meiotic double-strand break formation. *Genetics*, **173**, 1969–1981.
38. Sasanuma,H., Murakami,H., Fukuda,T., Shibata,T., Nicolas,A. and Ohta,K. (2007) Meiotic association between Spo11 regulated by Rec102, Rec104 and Rec114. *Nucleci Acids Res.*, **35**, 1119–1133.
39. Malone,R.E., Bullard,S., Hermiston,M., Rieger,R., Cool,M. and Galbraith,A. (1991) Isolation of mutants defective in early steps of meiotic recombination in the yeast *Saccharomyces cerevisiae*. *Genetics*, **128**, 79–88.
40. Menees,T.M. and Roeder,G.S. (1989) *MEI4*, a yeast gene required for meiotic recombination. *Genetics*, **123**, 675–682.
41. Wan,L., Niu,H., Futcher,B., Zhang,C., Shokat,K.M., Boulton,S.J. and Hollingsworth,N.M. (2008) Cdc28-Clb5 (CDK-S) and Cdc7-Dbf4 (DDK) collaborate to initiate meiotic recombination in yeast. *Genes Dev.*, **22**, 386–397.
42. Murakami,H. and Keeney,S. (2014) Temporospatial coordination of meiotic DNA replication and recombination via DDK recruitment to replisomes. *Cell*, **158**, 861–873.
43. Penedos,A., Johnson,A.L., Strong,E., Goldman,A.S., Carballo,J.A. and Cha,R.S. (2015) Essential and checkpoint functions of budding yeast ATM and ATR during meiotic prophase are facilitated by differential phosphorylation of a meiotic adaptor protein, Hop1. *PLoS ONE*, **10**, e0134297.
44. Subramanian,V.V., MacQueen,A.J., Vader,G., Shinohara,M., Sanchez,A., Borde,V., Shinohara,A. and Hochwagen,A. (2016) Chromosome synapsis alleviates Mek1-dependent suppression of meiotic DNA repair. *PLoS Biol.*, **14**, e1002369.
45. Chuang,C.-N., Cheng,Y.-H. and Wang,T.-F. (2012) Mek1 stabilizes Hop1-Thr318 phosphorylation to promote interhomolog recombination and checkpoint responses during yeast meiosis. *Nucleci Acids Res.*, **40**, 11416–11427.
46. Niu,H., Wan,L., Baumgartner,B., Schaefer,D., Loidl,J. and Hollingsworth,N.M. (2005) Partner choice during meiosis is regulated by Hop1-promoted dimerization of Mek1. *Mol. Biol. Cell*, **16**, 5804–5818.
47. San-Segundo,P.A. and Roeder,G.S. (1999) Pch2 links chromatin silencing to meiotic checkpoint control. *Cell*, **97**, 313–324.
48. Herruzo,E., Ontoso,D. and González-Arranz,S. (2016) The Pch2 AAA+ ATPase promotes phosphorylation of the Hop1 meiotic checkpoint adaptor in response to synaptonemal complex defects. *Nucleic Acids Res.*, **44**, 7722–7741.
49. Zanders,S. and Alani,E. (2009) The *pch2Δ*; mutation in Baker's yeast alters meiotic crossover levels and confers a defect in crossover interference. *PLoS Genet.*, **5**, e1000571.
50. Caryl,A.P., Armstrong,S.J., Jones,G.H. and Franklin,F.C.H. (2000) A homologue of the yeast *HOP1* gene is inactivated in the *Arabidopsis* meiotic mutant *asy1*. *Chromosoma*, **109**, 62–71.
51. Nonomura,K.I., Nakano,M., Murata,K., Miyoshi,K., Eiguchi,M., Miyao,A., Hirochika,H. and Kurata,N. (2004) An insertional mutation in the rice *PAIR2* gene, the ortholog of *Arabidopsis ASY1*, results in a defect in homologous chromosome pairing during meiosis. *Mol. Genet. Genomics*, **271**, 121–129.
52. Kim,Y., Rosenberg,S.C., Kugel,C.L., Kostow,N., Rog,O., Davydov,V., Su,T.Y., Dernburg,A.F. and Corbett,K.D. (2014) The chromosome axis controls meiotic events through a hierarchical assembly of HORMA domain proteins. *Dev. Cell*, **31**, 487–502.
53. Hollingsworth,N.M. and Byers,B. (1989) *HOP1*: a yeast meiotic pairing gene. *Genetics*, **121**, 445–462.
54. Zetka,M.C., Kawasaki,I., Strome,S. and Müller,F. (1999) Synapsis and chiasma formation in *Caenorhabditis elegans* require HIM-3, a meiotic chromosome core component that functions in chromosome segregation. *Genes Dev.*, **13**, 2258–2270.
55. Couteau,F. and Zetka,M. (2005) HTP-1 coordinates synaptonemal complex assembly with homolog alignment during meiosis in *C. elegans*. *Genes Dev.*, **19**, 2744–2756.
56. Martinez-Perez,E. and Villeneuve,A.M. (2005) HTP-1-dependent constraints coordinate homolog pairing and synapsis and promote chiasma formation during *C. elegans* meiosis. *Genes Dev.*, **19**, 2727–2743.
57. Aravind,L. and Koonin,E.V. (1998) The HORMA domain: a common structural denominator in mitotic checkpoints, chromosome synapsis and DNA repair. *Trends Biochem. Sci.*, **23**, 284–286.
58. Rosenberg,S.C. and Corbett,K.D. (2015) The multifaceted roles of the HORMA domain in cellular signaling. *J. Cell Biol.*, **211**, 745–755.
59. Lara-Gonzalez,P., Westhorpe,F.G. and Taylor,S.S. (2012) The spindle assembly checkpoint. *Curr. Biol.*, **22**, R966–R980.
60. Musacchio,A. (2015) The molecular biology of spindle assembly checkpoint signaling dynamics. *Curr. Biol.*, **25**, R1002–R1018.
61. Primorac,I. and Musacchio,A. (2013) Panta rhei: the APC/C at steady state. *J. Cell Biol.*, **201**, 177–189.
62. Mapelli,M. and Musacchio,A. (2007) MAD contortions: conformational dimerization boosts spindle checkpoint signaling. *Curr. Opin. Struct. Biol.*, **17**, 716–725.
63. De Antoni,A., Pearson,C.G., Cimini,D., Canman,J.C., Sala,V., Nezi,L., Mapelli,M., Sironi,L., Faretta,M., Salmon,E.D. *et al.* (2005) The Mad1/Mad2 complex as a template for Mad2 activation in the spindle assembly checkpoint. *Curr. Biol.*, **15**, 214–225.
64. Luo,X. and Yu,H. (2008) Protein metamorphosis: the two-state behavior of Mad2. *Structure*, **16**, 1616–1625.
65. Rosenberg,S.C. and Corbett,K.D. (2015) The multifaceted roles of the HORMA domain in cellular signaling. *J. Cell Biol.*, **211**, 745–755.
66. Sironi,L., Mapelli,M., Knapp,S., De Antoni,A., Jeang,K.-T. and Musacchio,A. (2002) Crystal structure of the tetrameric Mad1-Mad2 core complex: implications of a 'safety belt' binding mechanism for the spindle checkpoint. *EMBO J.*, **21**, 2496–2506.
67. Luo,X., Tang,Z., Rizo,J. and Yu,H. (2002) The Mad2 spindle checkpoint protein undergoes similar major conformational changes upon binding to either Mad1 or Cdc20. *Mol. Cell*, **9**, 59–71.
68. Luo,X., Fang,G., Coldiron,M., Lin,Y., Yu,H., Kirschner,M.W. and Wagner,G. (2000) Structure of the Mad2 spindle assembly checkpoint protein and its interaction with Cdc20. *Nat. Struct. Biol.*, **7**, 224–229.
69. Mapelli,M., Massimiliano,L., Santaguida,S. and Musacchio,A. (2007) The Mad2 conformational dimer: structure and implications for the spindle assembly checkpoint. *Cell*, **131**, 730–743.
70. Chen,R.-H., Shevchenko,A., Mann,M. and Murray,A.W. (1998) Spindle checkpoint protein Xmad1 recruits Xmad2 to unattached kinetochores. *J. Cell Biol.*, **143**, 283–295.
71. Sironi,L., Melixetian,M., Faretta,M., Prosperini,E., Helin,K. and Musacchio,A. (2001) Mad2 binding to Mad1 and Cdc20, rather than oligomerization, is required for the spindle checkpoint. *EMBO J.*, **20**, 6371–6382.
72. Shah,J.V., Botvinick,E., Bonday,Z., Furnari,F., Berns,M. and Cleveland,D.W. (2004) Dynamics of centromere and kinetochore proteins; implications for checkpoint signaling and silencing. *Curr. Biol.*, **14**, 942–952.
73. Chao,W.C.H., Kulkarni,K., Zhang,Z., Kong,E.H. and Barford,D. (2012) Structure of the mitotic checkpoint complex. *Nature*, **484**, 208–213.
74. Faesen,A.C., Thanasoula,M., Maffini,S., Breit,C., Müller,F., van Gerwen,S., Bange,T. and Musacchio,A. (2017) Basis of catalytic assembly of the mitotic checkpoint complex. *Nature*, **542**, 498–502.
75. Hara,M., Özkan,E., Sun,H., Yu,H. and Luo,X. (2015) Structure of an intermediate conformer of the spindle checkpoint protein Mad2. *Proc. Nat. Acad. Sci. U.S.A.*, **112**, 11252–11257.

76. Ye,Q., Rosenberg,S.C., Moeller,A., Speir,J.A., Su,T.Y. and Corbett,K.D. (2015) TRIP13 is a protein-remodeling AAA+ ATPase that catalyzes MAD2 conformation switching. *eLife*, **4**, 213.
77. Tipton,A.R., Wang,K., Oladimeji,P., Sufi,S., Gu,Z. and Liu,S.-T. (2012) Identification of novel mitosis regulators through data mining with human centromere/kinetochore proteins as group queries. *BMC Cell Biol.*, **13**, 15.
78. Wang,K., Sturt-Gillespie,B., Hittle,J.C., Macdonald,D., Chan,G.K., Yen,T.J. and Liu,S.-T. (2014) Thyroid hormone receptor interacting protein 13 (TRIP13) AAA-ATPase is a novel mitotic checkpoint-silencing protein. *J. Biol. Chem.*, **289**, 23928–23937.
79. Teichner,A., Eytan,E., Sitry-Shevah,D., Miniowitz-Shemtov,S., Dumin,E., Gromis,J. and Hershko,A. (2011) p31^{comet} promotes disassembly of the mitotic checkpoint complex in an ATP-dependent process. *Proc. Nat. Acad. Sci. U.S.A.*, **108**, 3187–3192.
80. Miniowitz-Shemtov,S., Eytan,E., Kaisari,S., Sitry-Shevah,D. and Hershko,A. (2015) Mode of interaction of TRIP13 AAA-ATPase with the Mad2-binding protein p31^{comet} and with mitotic checkpoint complexes. *Proc. Nat. Acad. Sci. U.S.A.*, **112**, 11536–11540.
81. Eytan,E., Wang,K., Miniowitz-Shemtov,S., Sitry-Shevah,D., Kaisari,S., Yen,T.J., Liu,S.-T. and Hershko,A. (2014) Disassembly of mitotic checkpoint complexes by the joint action of the AAA-ATPase TRIP13 and p31(comet). *Proc. Nat. Acad. Sci. U.S.A.*, **111**, 12019–12024.
82. Westhorpe,F.G., Tighe,A., Lara-Gonzalez,P. and Taylor,S.S. (2011) p31^{comet}-mediated extraction of Mad2 from the MCC promotes efficient mitotic exit. *J. Cell Sci.*, **124**, 3905–3916.
83. Kim,Y., Rosenberg,S.C., Kugel,C.L., Kostow,N., Rog,O., Davydov,V., Su,T.Y., Dernburg,A.F. and Corbett,K.D. (2014) The chromosome axis controls meiotic events through a hierarchical assembly of HORMA domain proteins. *Dev. Cell*, **31**, 487–502.
84. Khan,K., Madhavan,T.P.V., Kshirsagar,R., Boosi,K.N., Sadhale,P. and Muniyappa,K. (2013) N-terminal disordered domain of *Saccharomyces cerevisiae* Hop1 protein is dispensable for DNA binding, bridging, and synapsis of double-stranded DNA molecules but is necessary for spore formation. *Biochemistry*, **52**, 5265–5279.
85. Friedman,D.B., Hollingsworth,N.M. and Byers,B. (1994) Insertional mutations in the yeast *HOP1* gene: evidence for multimeric assembly in meiosis. *Genetics*, **136**, 449–464.
86. Kironmai,K.M., Muniyappa,K., Friedman,D.B., Hollingsworth,N.M. and Byers,B. (1998) DNA-binding activities of Hop1 protein, a synaptonemal complex component from *Saccharomyces cerevisiae*. *Mol. Cell. Biol.*, **18**, 1424–1435.
87. Tropea,J.E., Cherry,S. and Waugh,D.S. (2009) Expression and purification of soluble His(6)-tagged TEV protease. *Methods Mol. Biol.*, **498**, 297–307.
88. Hollingsworth,N.M. and Johnson,A.D. (1993) A conditional allele of the *Saccharomyces cerevisiae HOP1* gene is suppressed by overexpression of two other meiosis-specific genes: *RED1* and *REC104*. *Genetics*, **133**, 785–797.
89. Yang,M., Li,B., Liu,C.-J., Tomchick,D.R., Machius,M., Rizo,J., Yu,H. and Luo,X. (2008) Insights into Mad2 regulation in the spindle checkpoint revealed by the crystal structure of the symmetric Mad2 dimer. *PLoS Biol.*, **6**, e50.
90. Mapelli,M., Filipp,F.V., Rancati,G., Massimiliano,L., Nezi,L., Stier,G., Hagan,R.S., Confalonieri,S., Piatti,S., Sattler,M. *et al.* (2006) Determinants of conformational dimerization of Mad2 and its inhibition by p31^{comet}. *EMBO J.*, **25**, 1273–1284.
91. Fukuda,T., Daniel,K., Wojtasz,L., Toth,A. and Höög,C. (2010) A novel mammalian HORMA domain-containing protein, HORMAD1, preferentially associates with unsynapsed meiotic chromosomes. *Exp. Cell Res.*, **316**, 158–171.
92. DeAntoni,A., Sala,V. and Musacchio,A. (2005) Explaining the oligomerization properties of the spindle assembly checkpoint protein Mad2. *Philos. Trans. R. Soc. Lond., B, Biol. Sci.*, **360**, 637–647.
93. Ye,Q., Kim,D.-H., Dereli,I., Rosenberg,S.C., Hagemann,G., Herzog,F., Toth,A., Cleveland,D.W. and Corbett,K.D. (2017) The AAA+ ATPase TRIP13 remodels HORMA domains through N-terminal engagement and unfolding. *EMBO J.*, **36**, 2419–2434.
94. Roig,I., Dowdle,J.A., Toth,A., de Rooij,D.G., Jasin,M. and Keeney,S. (2010) Mouse TRIP13/PCH2 is required for recombination and normal higher-order chromosome structure during meiosis. *PLoS Genet.*, **6**, e1001062.
95. Miao,C., Tang,D., Zhang,H., Wang,M., Li,Y., Tang,S., Yu,H., Gu,M. and Cheng,Z. (2013) CENTRAL REGION COMPONENT1, a novel synaptonemal complex component, is essential for meiotic recombination initiation in rice. *Plant Cell*, **25**, 2998–3009.
96. Ma,H.T. and Poon,R.Y.C. (2016) TRIP13 regulates both the activation and inactivation of the spindle-assembly checkpoint. *Cell Rep.*, **14**, 1086–1099.